Journal of The Electrochemical Society, **157** (7) H721-H726 (2010)
0013-4651/2010/157(7)/H721/6/$28.00 © The Electrochemical Society

Hydride Vapor Phase Epitaxy Growth of Semipolar $(10\bar{1}\bar{3})$GaN on Patterned *m*-Plane Sapphire

T. B. Wei,[z] Q. Hu, R. F. Duan, X. C. Wei, J. K. Yang, J. X. Wang,[*] Y. P. Zeng, G. H. Wang, and J. M. Li

Semiconductor Lighting Technology Research and Development Center, Institute of Semiconductors, Chinese Academy of Sciences, Beijing 100083, China

We have investigated the hydride vapor-phase epitaxy growth of $(10\bar{1}\bar{3})$-oriented GaN thick films on patterned sapphire substrates (PSSs) $(10\bar{1}0)$. From characterization by atomic force microscopy, scanning electron microscopy, double-crystal X-ray diffraction, and photoluminescence (PL), it is determined that the crystalline and optical qualities of $(10\bar{1}\bar{3})$ GaN epilayers grown on the cylindrical PSS are better than those on the flat sapphire. However, two main crystalline orientations $(10\bar{1}\bar{3})$ and $(11\bar{2}2)$ dominate the GaN epilayers grown on the pyramidal PSS, demonstrating poor quality. After etching in the mixed acids, these $(10\bar{1}\bar{3})$ GaN films are dotted with oblique pyramids, concurrently lining along the $\langle 30\bar{3}\bar{2}\rangle$ direction, indicative of a typical N-polarity characteristic. Defect-related optical transitions of the $(10\bar{1}\bar{3})$ GaN epilayers are identified and detailedly discussed in virtue of the temperature-dependent PL. In particular, an anomalous blueshift–redshift transition appears with an increase in temperature for the broad blue luminescence due to the thermal activation of the shallow level.
 [DOI: 10.1149/1.3425820]

Manuscript submitted September 25, 2009; revised manuscript received April 8, 2010. Published May 10, 2010.

Today's *c*-plane quantum-well-based GaN optoelectronics suffer from a reduced radiative efficiency and a redshift of the optical transitions as a result of the polarization-induced Stark effect in quantum wells. To resolve these problems, the growth of GaN on a semipolar surface has also been attempted besides the nonpolar orientations. Recently, semipolar light emitting diodes grown on $(10\bar{1}1)$ and $(11\bar{2}2)$ templates sliced from thick $\langle 0001\rangle$-oriented bulk crystal grown by hydride vapor-phase epitaxy (HVPE) have been demonstrated with great potential in performance improvement.[1,2] However, these templates are very small, expensive, and not commercially available for mass production. Alternatively, the heteroepitaxy of semipolar GaN layers on low cost foreign substrates is a quite interesting option. So far, different semipolar GaN epitaxial layers, including $(10\bar{1}1)$, $(10\bar{1}\bar{3})$, and $(11\bar{2}2)$ crystalline planes, have already been grown on spinel substrates,[3,4] *m*-plane sapphire,[5-8] as well as silicon substrates by selective area growth.[9,10] However, the epitaxial growth of semipolar GaN remains challenging due to the strong anisotropy of the surface properties, resulting in epitaxial layers with a high density of crystalline defects, mainly basal stacking faults (BSFs) and threading dislocations.

Meanwhile, high quality *c*-plane GaN epitaxial layers with low dislocation densities can be achieved on maskless *c*-plane patterned sapphire substrates (PSSs) with periodic grooves or holes.[11-13] In comparison with the conventional epitaxial lateral overgrowth technique, the photolithography and epilayer growth process are simplified, and the contamination from the dielectric mask is prevented. In addition, the geometrical effect of patterned substrates can also effectively enhance light extraction, improving the optoelectronic device performance and efficiency. In this case, a promising alternative would be to get large, low defect density, and cost-effective semipolar GaN by using nonpolar PSSs. However, to our knowledge, research efforts on semipolar GaN have mainly focused on the $(11\bar{2}2)$ orientation. There are few works devoted to the epigrowth of $(10\bar{1}\bar{3})$-oriented GaN,[14,15] and detailed investigations on the growth conditions are still lacking.

In this work, we prepare the cylinder and pyramid PSSs using a hexagonal pattern on the *m*-plane sapphires with different etching times by wet chemical etching. The morphology, structural, and optical characteristics of $(10\bar{1}\bar{3})$ semipolar GaN epilayers grown on the *m*-plane PSSs and flat sapphire by HVPE are investigated. Furthermore, the optical emission properties of typical $(10\bar{1}\bar{3})$ GaN grown on the cylindrical PSS are detailedly discussed by temperature-dependent photoluminescence (PL) spectra.

Experimental

The sapphire substrates used in this study were 2 in. diameter, 430 μm thick, and on-axis (±0.1°) *m*-plane sapphire. For wet etching, 500 nm SiO_2 was deposited on sapphire by plasma-enhanced chemical vapor deposition. A hexagonal photoresist array with a 4 μm diameter and 2 μm spacing was defined by the standard photolithography process on SiO_2 film. Then, the SiO_2 film was patterned using reactive ion etching. After SiO_2 patterning, the photoresist was removed with a mixture of H_2SO_4 and H_2O_2 (H_2SO_4:H_2O_2 = 3:1), and the SiO_2 array was left to serve as the mask for the etching of sapphire substrates. A mixture of H_2SO_4:H_3PO_4 (2:1) solution was used to etch sapphire at 280°C. After etching sapphire, the SiO_2 mask was removed in dilute HF, and lastly sapphire substrates were rinsed in deionized water for 5 min and blown dry under nitrogen.

The patterned *m*-plane substrates were loaded into the home-designed vertical HVPE system. Before the growth, the nitridation treatment was carried out at 1050°C in NH_3 for 8 min, and subsequently GaCl treatment was carried out for 30 s to provide adequate nucleation centers. The epitaxial growths were performed at atmospheric pressure and at 1050°C, with a V/III ratio of about 22. The total flow rate of the N_2 carrier gas was fixed to 6 L/min. Finally, 70 μm thick GaN films were obtained on the *m*-plane PSSs in 1 h, with a corresponding growth rate of approximately 70 μm/h. To directly compare the quality of GaN on PSSs and flat sapphire, we also grew GaN layers under the same conditions on the unpatterned flat sapphire. The crystallographic orientation and the crystalline quality of the grown GaN films were studied by a Bede D1 high resolution triple axis diffractometer using Cu $K\alpha_1$ radiation. The surface morphology of the PSSs and the subsequent GaN thick films were characterized by JSM-5600LV scanning electronic microscope (SEM) and Nanoscope III atomic force microscope (AFM) operated in the tapping mode. Crystal polarity and defects characteristic of these semipolar films were determined by selective etching in a mixture of H_2SO_4 and H_3PO_4 (H_2SO_4:H_3PO_4 = 2:1) for 3 min at 280°C. Finally, temperature-dependent PL measurement excited with a 325 nm He–Cd laser was also performed from 5 to 290 K to

* Electrochemical Society Active Member.
[z] E-mail: tbwei@semi.ac.cn

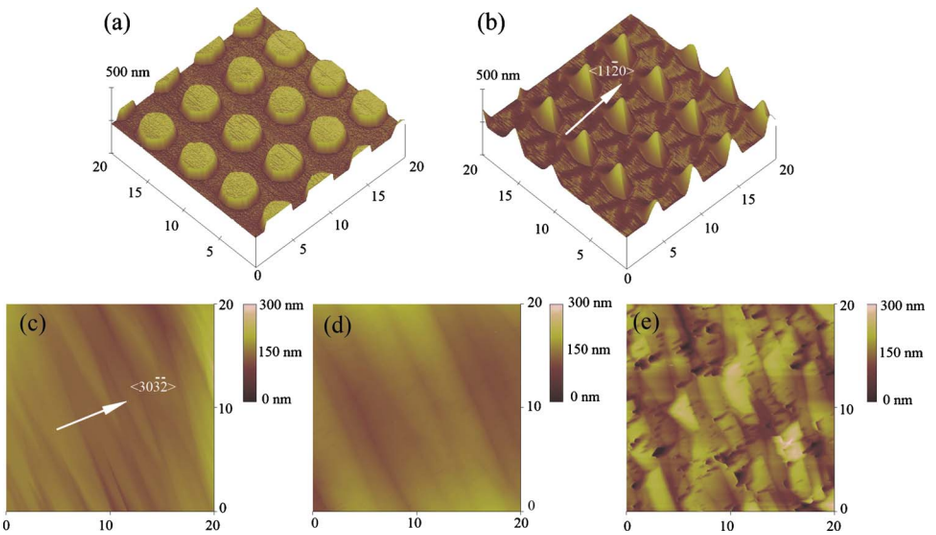

Figure 1. (Color online) AFM images of *m*-plane sapphire etched in $2H_2SO_4$:$1H_3PO_4$ mixture at 280°C for (a) 10 and (b) 60 min. Surface morphology of GaN grown by HVPE on (c) flat sapphire, (d) PSS with 10 min etching, and (e) PSS with 60 min etching.

investigate the optical property of the semipolar $(10\bar{1}\bar{3})$ GaN films. The PL signal was dispersed by a single-grating monochromator and was detected by a charge-coupled device camera.

Results and Discussion

Figure 1a and b shows the 20 × 20 μm AFM images of *m*-plane sapphire etched by H_2SO_4 and H_3PO_4 solutions under different etching times. As can be seen in the figure, cylindrical PSS is obtained with a regular distribution at 10 min etching. The height and the top surface diameter of the cylindrical pattern are 50 nm and 3.7 μm, respectively. When the etching time is increased to 60 min, the pyramidal pattern with a height of 240 nm is formed. This is attributed to the lateral overetching; namely the acids gradually attack the cylinder side facet with the increase in the etching depth. The higher etching rate along the $\langle 11\bar{2}0\rangle$ orientation can be clearly resolved in Fig. 1b, demonstrating in-plane anisotropic etching features of the *m*-plane sapphire substrate. In addition, when compared to the conventional *c*-plane sapphire, the *m*-plane sapphire shows a low etching rate of about 0.24 μm/h due to the different configuration of surface atoms and the bond structure. In contrast, the etching rate of *c*-plane sapphire reaches 6 μm/h under the same etching conditions.[11]

The surface morphology of $(10\bar{1}\bar{3})$ GaN epilayers grown on the above two types of PSSs and flat sapphire is shown in Fig. 1c-e. Like the previous nonpolar GaN results,[16,17] slatelike patterns, aligned perpendicular to the $[30\bar{3}\bar{2}]$ direction, are clearly observed on these semipolar film surfaces. Usually, the slate features are attributed to the intersections of basal-plane stacking faults with the growth surface, reflecting the density of BSFs.[18] Here, we can observe that the slate density of GaN on cylindrical PSS is lower than that of GaN on flat sapphire. Simultaneously, the root-mean-square roughness values of the GaN surface grown on the cylindrical PSS and flat sapphire are 11.8 and 13.4 nm for a 20 × 20 μm area, respectively. It is thus evidenced that the crystalline quality of the GaN epilayer may be improved via the later epitaxial overgrowth on a cylinder PSS.

On the contrary, the GaN film grown on the pyramidal PSS is dominated by the randomly distributed pits of 200–2000 nm, and the undulating morphology also becomes less prominent due to a high roughness of about 33.9 nm in Fig. 1e. In addition to the pits, large inclined hillocks are also found on the surface. The distinct morphology difference of GaN epilayers on the two types of PSSs may be ascribed to the effects of the patterns' shape and height. For the cylindrical PSS, the GaN film grows not only on the etched basal surface but also on the unetched mesas, whereas the growth of GaN on the pyramidal PSS is initiated only from the etched basal surface and then laterally propagates toward the sidewalls of the pyramids.[19] However, the migration lengths of adatoms along the nonpolar and semipolar directions are much lower than that along the *c*-direction, leading to the lower lateral growth rate on the *m*-sapphire.[20] Therefore, combining the relatively higher pattern height, incomplete coalescence occurs and poor GaN morphology is obtained on the pyramidal PSS. To obtain a smooth GaN epilayer on the pyramidal PSS, the growth conditions must be optimized again, such as increasing the temperature and changing the V/III ratio; further research work is being carried out.

Figure 2a presents X-ray diffraction (XRD) 2θ–ω scans in a symmetric configuration for the two types of GaN films grown on *m*-plane PSSs. For the rough GaN layer grown on the pyramidal

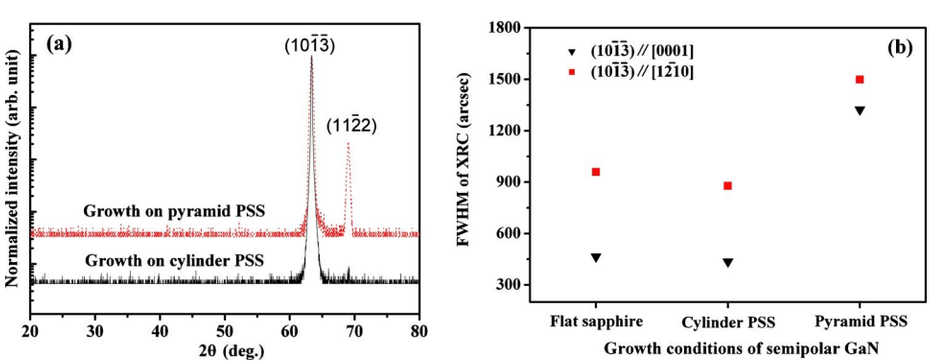

Figure 2. (Color online) (a) The 2θ–ω XRD scan and (b) symmetrical $(10\bar{1}\bar{3})$ X-ray rocking curves of semipolar GaN epilayers grown on the flat sapphire and two types of *m*-plane PSSs.

PSS, the X-ray reflections corresponding to GaN $(10\bar{1}\bar{3})$ and GaN $(11\bar{2}\bar{2})$ can be observed. The additional peak at $2\theta = 69.06°$ reveals the presence of GaN $\{11\bar{2}2\}$ domains in the film, which may be formed in the coalesced process. The polycrystalline characteristic agrees with recent reports of GaN epitaxy on *m*-sapphire,[21,22] which shows a competition between $(10\bar{1}\bar{3})$ and $(11\bar{2}\bar{2})$ domains depending on the growth conditions. However, similar to that grown on the flat sapphire, only one sharp GaN $(10\bar{1}\bar{3})$ peak can be seen within the detection limits of the XRD system for the film grown on the cylindrical PSS.

The crystallinity of semipolar GaN epilayers grown on a flat sapphire and two types of PSSs is examined by double-crystal XRD. The ω-scans of these films indicate notable anisotropy of the full width at half-maximum (fwhm) with respect to the direction of the incident X-ray beam, as often observed in nonpolar GaN. The trend in the crystal quality of different GaN films shows a good agreement with the results revealed by the AFM images. As shown in Fig. 2b, the fwhm values for $(10\bar{1}\bar{3})$ GaN grown on the flat sapphire are 465 and 958 arcsec along the $[0001]_{\text{sapphire}}$ and $[1\bar{2}10]_{\text{sapphire}}$ directions, respectively, whereas GaN grown on the cylinder PSS shows relatively lower fwhm's, only 436 and 877 arcsec measured according to the corresponding directions. These fwhm values are quite low compared with those reported for semipolar GaN grown on *m*-plane sapphire substrates so far,[8,21] indicative of the high crystalline quality of HVPE epilayers. Moreover, an inspection reveals that in comparing results of GaN on the flat sapphire, the cylindrical PSS may help to reduce the anisotropy of semipolar GaN, especially reducing the tilt mosaic along the sapphire $[1\bar{2}10]$ direction. In nonpolar and semipolar GaN, the anisotropic behavior is caused due to the anisotropic growth, most likely related to unavoidable defects with a specific distribution. Here, the lateral coherence on the cylinder PSS may limit the elongation of the surface stripe structure along the $[30\bar{3}\bar{2}]$ direction, which accommodates a high density of defects. Nevertheless, further study of the structural properties using methods such as transmission electron microscopy is necessary to clarify this point. As expected, GaN grown on the pyramidal PSS shows poor crystalline quality, with fwhm's of 1323 and 1499 arcsec measured parallel to the sapphire [0001] and $[1\bar{2}10]$ directions, respectively, when approximately denoted as $(10\bar{1}\bar{3})$-GaN.

Because XRD does not permit us to uniquely identify the polarity of the semipolar GaN epilayers, wet chemical etching was carried out using hot mixed H_3PO_4/H_2SO_4 solution. Presently, wet chemical etching is a fast and simple method to determine the density and distribution of defects and crystal polarity in *c*-plane GaN based on the principle of forming etch pits or protruding features in defect sites.[23] Figure 3 presents the SEM images of etched $(10\bar{1}\bar{3})$ GaN epilayers grown on the different substrates. After etching, the undulating stripes discussed above completely disappear, and the surface of these films is covered with many inclined pyramids, which illustrates that all the semipolar films are designated "N-face" according to the etching characteristic of N-polarity nitride semiconductors. Regardless of their sizes, all the pyramids have faceted rhombohedral sidewalls in the sixfold mode. The formation of the inclined pyramids indicates that the etching rate of the various planes is greatly different due to the strong anisotropy of the semipolar GaN wurtzite structure. For good quality GaN on the flat sapphire and cylinder substrate, all the pyramids have the same azimuthal orientation, concurrently lined along the $\langle 30\bar{3}\bar{2}\rangle$ direction, namely perpendicular to the surface stripes. In addition, the size of pyramids for GaN grown on cylinder PSS slightly increases, and the density of pyramids decreases to approximately 1.6×10^5 cm^{-2} when compared to that on flat sapphire with a density of 3.5×10^5 cm^{-2}. Usually, as nucleation points for the etching process, the threading dislocations as well as other defects are preferentially

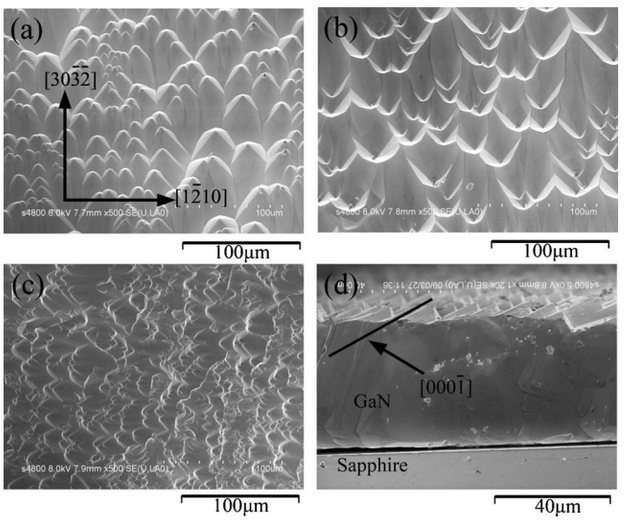

Figure 3. SEM surface images of etched semipolar films GaN grown on (a) flat sapphire, (b) cylinder PSS, and (c) pyramid PSS in H_2SO_4:H_3PO_4 (2:1) solution at 280°C for 3 min. (d) The corresponding cross-sectional view of etched GaN grown on the cylinder PSS.

etched. However, for the GaN on the pyramid PSS, many unorderly pyramids can be observed in Fig. 3c, demonstrating the polycrystalline characteristic and agreeing with the XRD result.

As shown from the cross-sectional view of an SEM micrograph in Fig. 3d, the angle between the $(10\bar{1}\bar{3})$ plane and the prolonged sidewalls of the pyramids is approximately 30°. According to (0002) reflection at a radial angle of 32° with respect to the substrate normal, we speculate that the longest tilted planes belong to $(000\bar{1})$ planes. Usually, anisotropic etching results in local surface decomposition under the formation of more stable facets. Thus, it is concluded that $(000\bar{1})$ surfaces have lower surface energies in comparison with other planes in the $(10\bar{1}\bar{3})$ semipolar GaN epilayer. In contrast, Gao et al. found that $\{10\bar{1}\bar{1}\}$ surfaces were the stable facets and etched slowly compared to the $(000\bar{1})$ surfaces in *c*-axis N-face GaN.[24] The origin of this discrepancy is still unclear, maybe due to the different initial growth planes, which usually contain many defects. In addition, a close examination reveals that partial separation occurs at the interface between the GaN epilayer and the PSS, but no hexagonal pyramids can be observed from the epilayer bottom close to the long slit, demonstrating the Ga-polarity characteristic. Here, the small voids near the interface, which are formed by the lateral coalescence of GaN on the PSS, are easier to contact with the acid solution and accelerate the etching process and separation.

Further evidence of the improvement of the semipolar film quality grown on the PSSs are observed in the PL measurement at 5 K. As shown in Fig. 4, all the spectra of $(10\bar{1}\bar{3})$ GaN films reveal four main emission bands that are located at about 3.47, 3.44, 3.33, and 3.29 eV. According to the previous results of nonpolar *a*-plane GaN,[25,26] the 3.47 eV emission may be ascribed to the common GaN near bandedge emission (NBE), the 3.44 eV emission to basal-plane stacking faults of type I_1, the 3.33 eV emission to the prismatic stacking faults intersecting the BSFs, and the 3.29 eV emission to the impurities incorporated in the partial dislocations. At lower energies, two phonon replicas of the 3.29 eV emission are also detected. When compared to the GaN grown on the flat sapphire, an obvious redshift in NBE peak energy from those grown on the cylinder and pyramid PSSs may be observed, around 3 and 5 meV, respectively. The redshift of the NBE in the GaN epilayers grown on the two types of PSSs may be attributed to a partial relief of compressive stress during the growth on the PSSs. On the contrary, it is

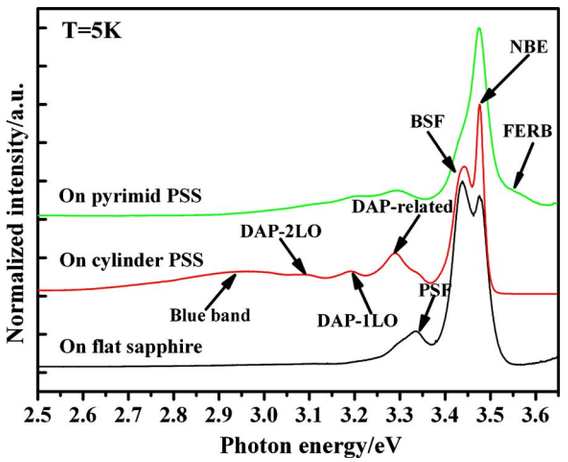

Figure 4. (Color online) Low temperature PL spectra of $(10\bar{1}\bar{3})$ GaN films grown on the flat sapphire and two types of *m*-plane PSSs.

surprising that the BSF-related peaks from the GaN on the flat sapphire and cylinder PSS are located at 3.436 and 3.441 eV, instead exhibiting a blueshift of about 5 meV. The anomalous behavior is similar to the results reported previously by Paskov et al.[25] that BSF-related emission may arise from bundles of BSFs. Having in mind the different spatial distribution of BSFs, the blueshift of 3.44 eV peak is comprehensible and does not reflect the strain variation of film.

Somewhat similar to the trend of the XRD results for different GaN layers, the fwhm's of the NBE peak of GaN grown on the flat sapphire, the cylindrical PSS, and the pyramidal PSS are 25, 18, and 38 meV, respectively. They also indicate that the crystalline quality of GaN grown on the cylinder PSS is better than that on flat sapphire. Simultaneously, for the GaN grown on flat sapphire, the NBE emission appears as a shoulder of the BSF-related peak, whereas the PL emission from the GaN grown on the cylinder PSS has been entirely dominated by NBE recombination due to a reduction in crystallographic defect density, especially BSFs. However, despite the poor quality, the relative intensity between the BSF-related emission and the NBE peak in GaN grown on the pyramid PSS is greatly reduced instead. It is thus reasonable to speculate that the polycrystalline mosaic structure in GaN epilayers grown on the pyramid PSS may inhibit the formation of BSFs. At high energy, an additional emission band can be seen at 3.55 eV for GaN on the pyramid PSS, which is treated as a free electron recombination across the bandgap.[27] Such spectra are typical of highly doped degraded semiconductor materials. Its origin may be related to the high concentration of donor impurities, such as nitrogen vacancies (V_N) in low quality GaN. In addition, a broad blue luminescence (BL) centered at 2.96 eV is only found in the semipolar GaN grown on the cylinder PSS. Unlike the notorious yellow band, the BL is not as commonly observed in the undoped GaN. It has been attributed to point defects, transmitting from the conduction band or shallow donor to a deep acceptor.[28] The assignment is discussed below in detail.

Finally, for more insight into the optical properties of $(10\bar{1}\bar{3})$ GaN, we performed a detailed study of the representative GaN film grown on the cylinder PSS with high quality by using temperature-dependent PL from 5 to 290 K. To clarify the temperature dependence of the observed PL lines, the normalized ratios of luminescence intensities are shown in Fig. 5a. These spectra clearly illustrate that there is an overall decrease in intensity and a shift to lower energy for the NBE with increasing temperature, as expected. The ratio of intensity between the NBE and 3.44 eV emission almost remains constant below 60 K. On the contrary, Paskov et al. found the BSF-related emission quenched quite faster than the NBE with increasing temperature in *a*-plane GaN.[25] Nevertheless, the 3.44 eV line also appears to be thermally quenched, namely turning into a shoulder above 40 K and absolutely disappearing above approximately 120 K, whereas the NBE peak is maintained up to room temperature and dominates the PL spectra all the way. Thus, the thermal quenching of 3.44 eV emission intensity is fitted by the well-known equation for the PL thermal quenching $I(T) = I(0)/[1 + \Sigma C_i \exp(-E_i/kT)]$, where $I(T)$ is the PL intensity, C is a fitting constant, E is the activation energy, and k is the Boltzmann constant. From the Arrhenius plot of the 3.44 eV emission intensity, we can extract thermal activation energies of 4 and 21 meV relevant to the low ($T \leq 30$ K) and high temperature ranges, respectively. The first low activation energy may correspond to the hole detrapping and be accounted for by assuming that the 3.44 eV peak arises from the recombination of excitons bound to some structural defects in semipolar GaN, such as I_1-type BSF. The second activation energy is due to the thermally induced electron delocalization from BSF at higher temperatures.

The 3.33 eV emission is rather weak in the temperature-dependent spectra and completely disappears above 60 K. The weakness of the 3.33 eV band prevents detailed study of the temperature dependence of its intensity and peak position. Likewise, the 3.29 eV emission is also found to quench with increasing temperature similar to stacking fault-related emissions. But, comparatively, the 3.29 eV peak intensity is instead enhanced with the increase in temperature relative to the NBE intensity up to 120 K, and then rapidly quenches and is hardly observable at 200 K. The quenching behavior of the band and its phonon replicas is like the conventional donor-acceptor pair (DAP) emission in *c*-axis GaN. However, the peak at 3.29 eV does not move gradually closer toward the bandgap but follows the bandgap variation as the temperature increases. Thus, it is tentatively concluded that the 3.29 eV peak in $(10\bar{1}\bar{3})$ GaN consists of two overlapping bands, including the defect-related emission and the usual DAP emission. These observations are in accordance with the results of *a*-plane GaN grown by metallorganic chemical vapor deposition (MOCVD).[25,29]

With increasing temperature, the absolute intensity of broad

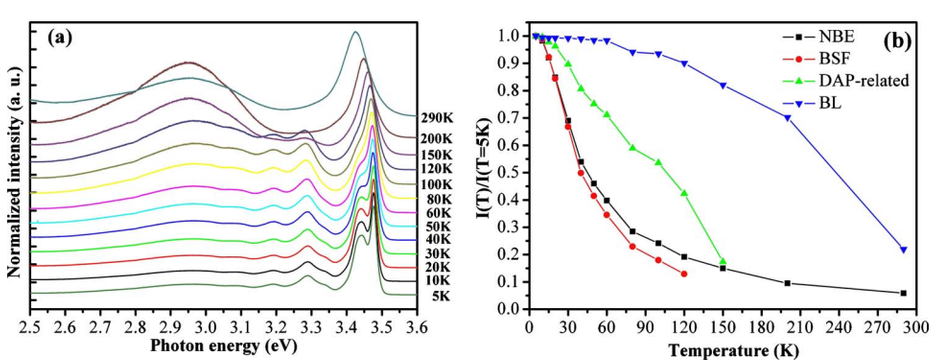

Figure 5. (Color online) Temperature dependence of (a) PL spectra from the typical semipolar GaN epilayer grown on cylindrical PSS and (b) the normalized PL intensity of NBE-, BSF-, and DAP-like emissions and blue band.

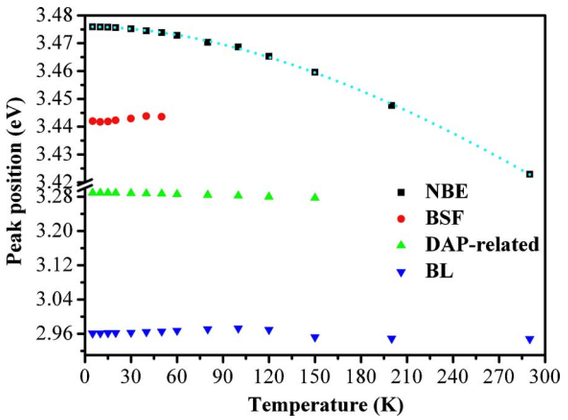

Figure 6. (Color online) The peak energies of NBE-, BSF-, DAP-related emissions and BL from the semipolar GaN grown on the cylindrical PSS as a function of temperature. The dotted curve represents the best fits of NBE energy positions with Varshni's semiempirical model.

BL almost remains constant up to 60 K and then slowly decreases compared to other emissions in Fig. 5b. Additionally, the BL peak becomes stronger in intensity relative to the NBE as the temperature is increased and begins to rapidly weaken above 200 K. The thermal quenching of the BL intensity is fitted by $I(T) = I(0)/[1 + C\ \exp(-E_A/kT)]$. Thus, the calculated activation energy from the Arrhenius plots is about 130 meV for the BL. This is the thermal ionization energy of the acceptor involved in the BL. Above 200 K, the PL quenching is attributed to the thermal release of trapped holes from the acceptor level to the valence band. However, the origin of the deep acceptor involved in the BL is still uncertain. For these undoped semipolar GaN epilayers, the magnesium or carbon acceptor impurities may be ruled out. Here, the BL is not found in GaN grown on the flat sapphire and pyramid PSS but only appears in GaN on the cylinder PSS. Therefore, we speculate that the BL may be caused by an excess of gallium vacancy V_{Ga} and its complexes with Si and O impurities, which originate from the remnants of the SiO_2 mask on the cylinder top surface.[30] In contrast, the hexagonal SiO_2 mask on the pyramid PSS has been eliminated during the excessive lateral overetching of sapphire, along with the formation of the pyramid pattern. Further investigation needs to be carried out to clarify the reason.

The peak energies of the NBE-, BSF-, and DAP-related bands as well as BL as a function of temperature are displayed in Fig. 6. The temperature-dependent energy gap follows Varshni's equation, $E_g(T) = E_g(0) - \alpha T^2/(\beta + T)$, where $E_g(T)$ is the transition energy at temperature T, $E_g(0)$ is the corresponding energy at 0 K, and α and β are known as Varshni's thermal coefficients and the Debye temperature, respectively. Given that the binding energy of the NBE is nearly independent of the temperature, we obtain the best fit for $E_g(0) = 3.476$ eV, $\alpha = 6.3 \times 10^{-4}$ eV/K, and $\beta = 710$ K. These values reasonably agree with the recently reported values for *c*- and *a*-plane GaN within the error.[25,31] Nevertheless, BSF- and DAP-related bands and BL could not be fitted properly using this formula because deep levels are involved in these bands. The BSF energy position follows a typical "S-shaped" temperature dependence, whereas the DAP-related emission shows a monotonic decrease in peak energy with an increase in temperature, resembling the trend of the bandgap shrinkage except for the minor difference in curve shape. The S-shaped behavior is also indicative of the fact that the 3.44 eV emission arises from localized excitons/carriers, which are bounded in the stacking faults. The initial blueshift and small activation energy of 4 meV correspond to the exciton thermal delocalization.

The energy position of BL exhibits a nonmonotonic dependence on the temperature. The BL peak first blueshifts by about 12 meV until 100 K and then redshifts following the bandgap shrinkage. In contrast, a redshift of nearly 15 meV occurs as the temperature is increased from 13 to 150 K for the BL in carbon-doped GaN grown by MOCVD.[32] This suggests that the origin of the BL in our study is different from the one in that case. At low temperatures, we think that the shift to the higher energies for BL is due to the progressive enhancement of the free-to-bound transition after the thermal activation of the shallow level. Here, some localized electrons are possibly activated from the shallow donor level, not holes from the deep acceptor level. At higher temperatures above 100 K, the recombination of delocalized states dominates the PL, and the peak energy of BL follows the delocalized exciton emission energy and thus decreases with the thermal shrinkage of gap energy.

Conclusion

$(10\bar{1}\bar{3})$ semipolar GaN thick films have been grown by HVPE on the PSSs $(10\bar{1}0)$. It is revealed that high quality $(10\bar{1}\bar{3})$ GaN is obtained on the cylindrical PSS, whereas the $(11\bar{2}2)$ impurity phase is introduced for the GaN grown on the pyramidal PSS. The semipolar GaN grown on the cylinder PSS shows narrow fwhm's of double-crystal XRD and PL spectra on a smooth surface when compared with that on the flat sapphire, illustrating an improved crystalline quality. For $(10\bar{1}\bar{3})$ GaN, many oblique pyramids cover the film surface after etching in the mixed acids and concurrently line along the $\langle 30\bar{3}\bar{2}\rangle$ direction, indicative of its N-polarity characteristic. According to the temperature-dependent PL, the 3.44 eV emission related to BSFs reveals thermal quenching with two activation energies (4 and 21 meV) and S-shaped temperature dependence of the peak position. Unlike the monotonic decrease in a peak energy of 3.29 eV emission, the 2.96 broad band shows a blueshift–redshift transition with an increase in temperature due to the thermal activation of the shallow level. The 2.96 band can only be found from GaN on the cylinder PSS, which may be produced by an excess of gallium vacancy V_{Ga} and its complexes with Si and O impurities, originating from the remnants of the SiO_2 mask.

Acknowledgments

This work was supported by the National High Technology Program of China under grant no. 2006AA03A143, the National Natural Sciences Foundation of China under grant no. 60806001, and the Knowledge Innovation Program of the Chinese Academy of Sciences under grant no. ISCAS2008T03.

Chinese Academy of Sciences assisted in meeting the publication costs of this article.

References

1. M. Funato, M. Ueda, Y. Kawakami, Y. Narukawa, T. Kosugi, M. Takahashi, and T. Mukai, *Jpn. J. Appl. Phys., Part 2*, **45**, L659 (2006).
2. H. Zhong, A. Tyagi, N. N. Fellows, F. Wu, R. B. Chung, M. Saito, K. Fujito, J. S. Speck, S. P. DenBaars, and S. Nakamura, *Appl. Phys. Lett.*, **90**, 233504 (2007).
3. T. J. Baker, B. A. Haskell, F. Wu, P. T. Fini, J. S. Speck, and S. Nakamura, *Jpn. J. Appl. Phys., Part 2*, **44**, L920 (2005).
4. J. F. Kaeding, M. Iza, H. Sato, S. P. DenBaars, J. S. Speck, and S. Nakamura, *Jpn. J. Appl. Phys., Part 2*, **45**, L536 (2006).
5. X. Ni, U. Ozgur, A. A. Baski, H. Morkoç, L. Zhou, D. J. Smith, and C. A. Tran, *Appl. Phys. Lett.*, **90**, 182109 (2007).
6. T. B. Wei, R. F. Duan, J. X. Wang, J. M. Li, Z. Q. Huo, J. K. Yang, and Y. P. Zeng, *Jpn. J. Appl. Phys.*, **47**, 3346 (2008).
7. R. Armitage and H. Hirayama, *Appl. Phys. Lett.*, **92**, 092121 (2008).
8. T. K. Zhu, D. Martin, and N. Grandjean, *Jpn. J. Appl. Phys.*, **48**, 020226 (2009).
9. N. Sawaki, T. Hikosaka, N. Koide, S. Tanaka, Y. Honda, and M. Yamaguchi, *J. Cryst. Growth*, **311**, 2867 (2009).
10. N. Suzuki, T. Uchida, T. Tanikawa, T. Hikosaka, Y. Honda, M. Yamaguchi, and N. Sawaki, *J. Cryst. Growth*, **311**, 2875 (2009).
11. D. S. Wuu, W. K. Wang, K. S. Wen, S. C. Huang, S. H. Lin, R. H. Horng, Y. S. Yu, and M. H. Pan, *J. Electrochem. Soc.*, **153**, G765 (2006).
12. K. T. Lee, Y. C. Lee, and J. Y. Chang, *J. Electrochem. Soc.*, **155**, H673 (2008).
13. T. V. Cuong, H. S. Cheong, H. G. Kim, H. Y. Kim, C. H. Hong, E. K. Suh, H. K. Cho, and B. H. Kong, *Appl. Phys. Lett.*, **90**, 131107 (2007).
14. R. Sharma, P. M. Pattison, H. Masui, R. M. Farrell, T. J. Baker, B. A. Haskell, F. Wu, S. P. DenBaars, J. S. Speck, and S. Nakamura, *Appl. Phys. Lett.*, **87**, 231110 (2005).

15. T. B. Wei, Q. Hu, R. F. Duan, X. C. Wei, Z. Q. Huo, J. X. Wang, Y. P. Zeng, G. H. Wang, and J. M. Li, *J. Cryst. Growth*, **311**, 4153 (2009).
16. C. Q. Chen, M. E. Gaevski, W. H. Sun, E. Kuokstis, J. P. Zhang, R. S. Q. Fareed, H. M. Wang, J. W. Yang, G. Simin, and M. A. Khan, *Appl. Phys. Lett.*, **81**, 3194 (2002).
17. R. Armitage, M. Horita, J. Suda, and T. Kimoto, *J. Appl. Phys.*, **101**, 033534 (2007).
18. B. A. Haskell, F. Wu, M. D. Graven, S. Matsuda, P. T. Fini, T. Fujii, K. Fujito, S. P. DenBaars, J. S. Speck, and S. Nakamura, *Appl. Phys. Lett.*, **83**, 644 (2003).
19. J.-H. Lee, J. T. Oh, Y. C. Kim, and J.-H. Lee, *IEEE Photonics Technol. Lett.*, **20**, 1563 (2008).
20. X. Ni, Y. Fu, Y. T. Moon, N. Biyikli, and H. Morkoç, *J. Cryst. Growth*, **290**, 166 (2006).
21. T. J. Baker, B. A. Haskell, F. Wu, J. S. Speck, and S. Nakamura, *Jpn. J. Appl. Phys., Part 2*, **45**, L154 (2006).
22. L. Lahourcade, J. Renard, B. Gayral, E. Monroy, M. P. Chauvat, and P. Ruterana, *J. Appl. Phys.*, **103**, 093514 (2008).
23. D. Zhuang and J. H. Edgar, *Mater. Sci. Eng., R.*, **48**, 1 (2005).
24. Y. Gao, T. Fujii, R. Sharma, K. Fujito, S. P. Denbaars, S. Nakamura, and E. L. Hu, *Jpn. J. Appl. Phys., Part 2*, **43**, L637 (2004).
25. P. P. Paskov, R. Schifano, B. Monemar, T. Paskova, S. Figge, and D. Hommel, *J. Appl. Phys.*, **98**, 093519 (2005).
26. R. Liu, A. Bell, F. A. Ponce, C. Q. Chen, J. W. Yang, and M. A. Khan, *Appl. Phys. Lett.*, **86**, 021908 (2005).
27. B. Arnaudov, T. Paskova, E. M. Goldys, S. Evtimova, and B. Monemar, *Phys. Rev. B*, **64**, 045213 (2001).
28. M. A. Reshchikov, F. Shahedipour, R. Y. Korotkov, B. W. Wessels, and M. P. Ulmer, *J. Appl. Phys.*, **87**, 3351 (2000).
29. T. Gühne, Z. Bougrioua, S. Laügt, M. Nemoz, P. Vennéguès, B. Vinter, and M. Leroux, *Phys. Rev. B*, **77**, 075308 (2008).
30. M. Toth, K. Fleischer, and M. R. Phillips, *Phys. Rev. B*, **59**, 1575 (1999).
31. I. Vurgaftman and J. R. Meyer, *J. Appl. Phys.*, **94**, 3675 (2003).
32. R. Armitage, Q. Yang, and E. R. Weber, *J. Appl. Phys.*, **97**, 073524 (2005).